
HydraMix: Multi-Image Feature Mixing for Small Data Image Classification

Christoph Reinders Frederik Schubert Bodo Rosenhahn
Institute for Information Processing / L3S, Leibniz University Hannover

Abstract

Training deep neural networks requires datasets with a large number of annotated examples. The collection and annotation of these datasets is not only extremely expensive but also faces legal and privacy problems. These factors are a significant limitation for many real-world applications. To address this, we introduce HydraMix, a novel architecture that generates new image compositions by mixing multiple different images from the same class. HydraMix learns the fusion of the content of various images guided by a segmentation-based mixing mask in feature space and is optimized via a combination of unsupervised and adversarial training. Our data augmentation scheme allows the creation of models trained from scratch on very small datasets. We conduct extensive experiments on ciFAIR-10, STL-10, and ciFAIR-100. Additionally, we introduce a novel text-image metric to assess the generality of the augmented datasets. Our results show that HydraMix outperforms existing state-of-the-art methods for image classification on small datasets.

1. Introduction

Pretraining on large datasets has led to state-of-the-art results in computer vision and machine learning (Krizhevsky et al., 2012). However, the size of these datasets makes them difficult to maintain, i.e., their labeling process is costly and difficult for new applications. This results in several problems regarding the privacy of individuals (Yang et al., 2020), unclear copyright claims (Henderson et al., 2023), and the resources required to use them (Bommasani et al., 2021). With transfer learning (Neyshabur et al., 2020), i.e., fine-tuning of models that have been pretrained on such a large dataset, it is possible to circumvent the resource issue. Nevertheless, this approach leaves the legal concerns open and also makes the users of such pretrained models dependent on companies or institutions that can afford to train them (Sharir et al., 2020). Thus, the research on making deep learning approaches work using only a small amount of data is vital.

One solution to achieving good performance with little data lies in combinatorics. Even with a handful of examples, it is possible to combine them in effectively infinitely different ways to enable the successful training of current machine learning pipelines with the augmented dataset. In image classification, several ways exist to mix multiple images using approaches ranging from simple image manipulations (Zhang et al., 2018) to methods that apply saliency guidance (Dabouei et al., 2021) to create combinations that resemble real objects more closely. However, simple methods are not able to create sensible combinations of the given objects, i.e., combinations that resemble real objects from the class or some sub-class. Moreover, the more complex methods fail in the small data regime due to the limited number of samples.

In this work, we present HydraMix, a method that is able to create meaningful combinations of images given only a handful of data samples without any pretraining. This work extends our conference article on the ChimeraMix method (Reinders et al., 2022), which learns to combine the features of two images guided by a mask before decoding them into a new image. The contributions of the original publication are:

- We propose a generative approach for addressing the small data image classification task.
- Our generator introduces a feature-mixing architecture for combining two images. Guided by a mask, the generator learns to combine image pairs.
- Experiments on benchmark datasets demonstrate that ChimeraMix outperforms previous methods in small data image classification.

HydraMix advances the ChimeraMix pipeline to its full combinatorial potential and introduces a feature-mixing architecture for combining an arbitrary number of images guided by a segmentation-based mixing mask. Our new proposed method establishes a new state of the art in small data image classification. Additionally, we present extensive ablation studies for crucial design choices of the pipeline and introduce a novel metric to assess the quality of data augmentation methods. An overview of HydraMix is shown

in Figure 1. In summary, our **contributions** in this work are:

- A novel architecture for mixing the content of an arbitrary number of images to generate new image compositions.
- HydraMix enables state-of-the-art image classification performance on small datasets.
- Enhancement of the mixing protocol for better sample quality.
- A new CLIP Synset Entropy evaluation to analyze the generalization capabilities of the generated images when using HydraMix.
- Extensive analysis of the primary hyperparameters and ablation studies.

2. Related Work

Training deep neural networks with only a handful of samples requires extensive regularization to prevent overfitting. Much research has already been put into the problem through general regularization methods, data augmentation, and, in particular, mixing pipelines. This section gives a brief overview of the three areas of research and provides a context of related work for our method.

2.1. Regularization for Small Data Problems

Small data problems pose a unique challenge where each part of the standard machine learning pipeline has to be adapted. Barz & Denzler (2020a) propose to use a cosine loss function instead of the commonly used cross-entropy loss to prevent the logits for one class from dominating the others. The convolutional neural tangent kernel (CNTK) has been used in (Arora et al., 2020) to study the behavior of ResNets on small datasets. Other models, such as Random Forests (Breiman, 2001), are less prone to overfitting on small datasets. This characteristic has been used by (Reinders et al., 2018) by combining them with neural networks to learn robust classifiers. Finally, Wavelet filters (Vetterli & Herley, 1992) have also been proposed in (Gauthier et al., 2021) to classify images given only a handful of samples.

Since we are in the small data regime without any pretraining, we can not rely on models such as StableDiffusion (Rombach et al., 2022) etc. that produce novel samples. Approaches such as GLICO (Azuri & Weinshall, 2021) use a Generative Adversarial Network (GAN) to synthesize novel images, but this task of modeling the data distribution is aggravated by the restriction to only a few samples. Instead, the data augmentation acts as a regularization for the model.

2.2. Data Augmentation

Synthetic samples can be created from a given set of images by randomly transforming each image. Random cropping and vertical or horizontal flipping are commonly used to prevent the model from focusing on a specific absolute location of a feature in an image (Krizhevsky et al., 2012). Other methods such as Cutout (DeVries & Taylor, 2017) or RandomErasing (Zhong et al., 2020) replace parts of the image with zeros or random noise. The specific hyperparameters of the data augmentation pipeline can be finetuned to a dataset as with AutoAugment (Cubuk et al., 2019) or sampled randomly, such as with the TrivialAugment (Müller & Hutter, 2021) method. Large models profit most from synthetically increasing the dataset size as they are more prone to overfitting (Brigato & Iocchi, 2021; Bornschein et al., 2020).

One natural way of extending the size of a small image dataset is the combination or mixing of two or more images to create novel variations of the data.

2.3. Mixing Augmentation

A central method that uses multiple image-label pairs to create convex combinations of them is MixUp (Zhang et al., 2018). The method has been extended to mix the samples in a learned feature space in (Verma et al., 2019). Since not all regions are equally suitable to be mixed, there are several methods that use the saliency of another model to guide the mixing process (Jeong et al., 2021; Kim et al., 2020; Dabouei et al., 2021; Kang & Kim, 2023). Another commonly used method is CutMix (Yun et al., 2019), where a rectangular region in one image is replaced by the content of another image from the same class. Liang et al. (2023) propose a system to apply mixing different transforms randomly that is similar to the random image transformations. For a comprehensive overview and benchmark of different mixing augmentations, see Li et al. (2023). In contrast to the presented methods above, we propose a pipeline based on the simple principle of combining multiple samples with a powerful generator that is able to create novel samples.

3. Method

In this work, we present HydraMix, a method for generating new image compositions from an arbitrary number of images in the small data regime, and establish a new state of the art on a set of datasets. Our method builds on the ChimeraMix (Reinders et al., 2022) approach and generalizes it to an arbitrary number of images.

The goal of our method is the generation of novel images by combining the semantic content of multiple images. Its main structure follows an encoder-decoder architecture similar to the CycleGAN architecture (Zhu et al., 2017) that is

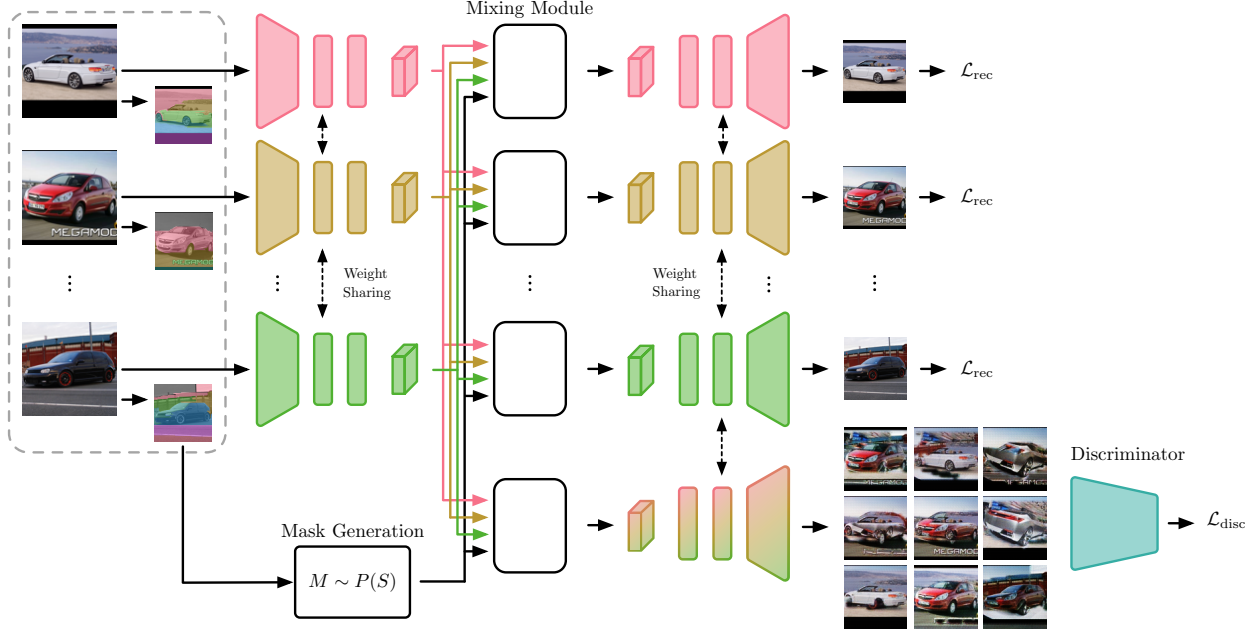


Figure 1: HydraMix introduces a novel feature-mixing architecture that combines the content of an arbitrary number of images in a feature space guided by a segmentation-based mixing mask. The model is optimized with reconstruction and adversarial losses. Afterward, HydraMix enables the generation of a large variety of new image compositions by sampling images and mixing masks.

trained adversarially using a discriminator. An overview of HydraMix is shown in Figure 1. In the following sections, the model architectures of the generator and discriminator, the mixing module, and the training are presented.

3.1. Encoder

While techniques such as MixUp (Zhang et al., 2018) work in pixel space, the experiments in (Reinders et al., 2022) have shown that it is beneficial to mix the images on a more abstract level in a learned feature space. Thus, the first component of the HydraMix generator is a convolutional encoder that maps the set of N images $\mathbf{I} \in \mathbb{R}^{N \times C_{in} \times H \times W}$ with C_{in} channels and a size of $H \times W$ to a lower dimensional feature map $\mathbf{F} \in \mathbb{R}^{N \times C_f \times H' \times W'}$ with C_f channels and a size of $H' \times W'$. For the sake of simplicity, we omit the index for the batch. The encoder consists of a block followed by N_{down} convolutional blocks with a stride of 2, which downsample the features and increase the number of features. Each convolutional block consists of a 2D convolution, normalization, and ReLU activation. In all our normalization layers, we use instance normalization to align the features adaptively. Finally, the encoder has $N_{blocks,enc}$ residual blocks. Note that this feature map retains some of the spatial information in order to allow for the subsequent mixing.

3.2. Mixing Module

The features are mixed guided by a mask so that each spatial region is filled with the features of a different image. HydraMix uses a segmentation-based mask generation where the images are segmented using the Felzenszwalb algorithm (Felzenszwalb & Huttenlocher, 2004). The resulting segmentations for all images are represented as $\mathbf{S} \in \mathbb{Z}^{N \times H \times W}$, where $S_{i,y,x}$ indicates the segmented region for each position. The segmentations are downsampled to the size of the features $\mathbf{S}' \in \mathbb{Z}^{N \times H' \times W'}$ using nearest neighbor interpolation.

In the next step, we generate a mixing mask $\mathbf{M} \in [0, 1]^{N \times H' \times W'}$ with $\sum_{i=1}^N M_{i,h,w} = 1 \forall h \in [1, H'], w \in [1, W']$. The mask is initialized with $M_{n,h,w} = \delta_{n,1}$, where δ is the Kronecker delta function. For each image $i \in [1, N]$, the set of all segments is defined as $\bar{S}_i = \{s \in \mathbb{Z} \mid \exists h \exists w : S'_{i,h,w} = s\}$. We randomly select segment regions from the current image by sampling a subset $\bar{S}_{i,sampled} \subseteq \bar{S}_i$, whereas each segment is included with a probability of 50%. The mask is updated to the selected segments by setting $M_{n,h,w} = \delta_{n,i}$ for all h and w if $S'_{i,h,w} \in \bar{S}_{i,sampled}$.

The mask values in our model are discrete, with each $M_{i,h,w}$ being an element of the set $\{0, 1\}$. We explored the possibility of generating continuous mask values by introducing

a blend factor for each image. However, this approach was ultimately less effective than discrete masks, as the latter yielded superior performance in our evaluations.

There are several ways of generating the mixing masks. In preliminary experiments, we determined that the segmentation-based sampling method shows better results than the grid-sampling method (ChimeraMix+Grid) when applied to more than two images. Thus, after generating the *segmentation*-based mixing mask, we calculate the mixed feature $\mathbf{F}_{\text{mix}} \in \mathbb{R}^{C_f \times H' \times W'}$ that combines the features of N images as follows

$$\mathbf{F}_{\text{mix}} = \sum_{i=1}^N \mathbf{F}_i \odot \mathbf{M}_i, \quad (1)$$

where \odot is the element-wise multiplication.

3.3. Decoder

Finally, the mixed features are passed to a convolutional decoder that maps from the feature space back to the pixel space. The design of the decoder is asymmetric to the encoder. The decoder consists of $N_{\text{blocks,dec}}$ residual blocks followed by N_{down} transposed convolution blocks that up-scale the features. At the end, a projection layer transforms the features to the image dimension C_{in} , producing the generated image $\hat{\mathbf{I}} \in \mathbb{R}^{C_{\text{in}} \times H \times W}$.

3.4. Discriminator

The discriminator receives the original and generated images as input and has the task of distinguishing the real from the fake images. The discriminator network has four convolutional blocks for extracting features. Each convolutional block consists of a 2D convolutional layer, normalization layer, and LeakyReLU activation. The convolutional layers, except for the first layer, have a stride of two to down-scale the features. Afterward, an output convolutional layer projects the features to a one-channel feature map followed by a Sigmoid activation. The generator and discriminator are trained adversarially, which will be explained in the next section.

3.5. Training

The generator $\text{Gen}(\mathbf{I}, \mathbf{M})$ combines the encoder Enc , mixing module Mix , and decoder Dec to produce the generated image $\hat{\mathbf{I}}$,

$$\hat{\mathbf{I}} = \text{Gen}(\mathbf{I}, \mathbf{M}) = \text{Dec}(\text{Mix}(\text{Enc}(\mathbf{I}), \mathbf{M})), \quad (2)$$

based on the input images \mathbf{I} and mixing mask \mathbf{M} .

To enable the generation of novel images from only a handful of samples, HydraMix uses multiple loss terms. When the mixing module receives a mask $\mathbf{M}^{\text{rec},i}$ which selects

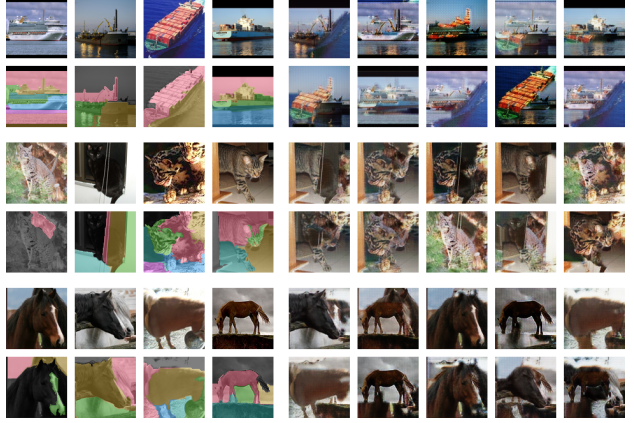


Figure 2: Qualitative samples using the HydraMix method on three classes from the STL-10 dataset. For each class, four original images and their segmentation masks (left) and ten generated image compositions (right) are shown.

only the features of one of the images, i.e., $\mathbf{M}_{j,h,w}^{\text{rec},i} = \delta_{j,i}$, a reconstruction loss and a perceptual loss are applied. The reconstruction loss \mathcal{L}_{rec} averages the mean squared error between the original image and the generated images over all N images with the respective mask $\mathbf{M}^{\text{rec},i}$, i.e.,

$$\mathcal{L}_{\text{rec}} = \frac{1}{NCHW} \sum_{i=1}^N \|\text{Gen}(\mathbf{I}, \mathbf{M}^{\text{rec},i}) - \mathbf{I}_i\|_2^2. \quad (3)$$

The visual appearance of the generated samples is improved by using a perceptual laplacian pyramid loss \mathcal{L}_{per} (Denton et al., 2015). The laplacian pyramid $L^l(\mathbf{X})$ at level l of an image \mathbf{X} is defined as the difference between the image downsampled $l-1$ times and the image downsampled l times and upsampled again once:

$$L^l(\mathbf{X}) = \mathbf{X} \downarrow_{l-1} - \mathbf{X} \downarrow_l \uparrow, \quad (4)$$

where \downarrow is the downsampling operator and \uparrow the upsample operator. The downsample and upsample operators are both implemented using a convolution. The laplacian pyramid loss is calculated by averaging the l_1 norm of the difference between the laplacian pyramid at level l of the generated image and the original images over L levels. We compute the perceptual loss for two images per batch to reduce the computational requirements when training our method:

$$\mathcal{L}_{\text{per}} = \frac{1}{N} \sum_{i=1}^N \sum_{l=1}^L \frac{1}{N_l} \|L^l(\text{Gen}(\mathbf{I}, \mathbf{M}^{\text{rec},i})) - L^l(\mathbf{I}_i)\|_1 \quad (5)$$

where N_l is the number of elements of $L^l(\mathbf{I}_i)$. This loss replaces the commonly used VGG (Simonyan & Zisserman, 2015) feature losses that are common when more data or pretrained networks are available.

Table 1: Test accuracy on ciFAIR-10, STL-10, and ciFAIR-100 with different numbers of samples per class for training comparing a standard classification baseline (Zagoruyko & Komodakis, 2016; He et al., 2016) as well as state-of-the-art methods for small data image classification, i.e., Cutout (DeVries & Taylor, 2017), Random Erasing (Zhong et al., 2020), Cosine (Barz & Denzler, 2020a), MixUp (Zhang et al., 2018), MixUpN†(Zhang et al., 2018), Scattering (Gauthier et al., 2021), GLICO (Azuri & Weinsall, 2021), ChimeraMix+Grid (Reinders et al., 2022), ChimeraMix+Seg (Reinders et al., 2022), and SuperMix (Dabouei et al., 2021). The best result is highlighted in bold. Note, that the size of the dataset of ciFAIR-100 with 5 samples per class is the same as that of ciFAIR-10 and STL-10 with 50 samples. †MixUpN is an extension of MixUp to multiple images by sampling the weighting from a Dirichlet distribution.

Samples per Class		5	10	20	30	50	100
Dataset	Method						
ciFAIR-10	Baseline	31.37±3.28	38.09±1.34	47.50±2.09	53.19±0.60	58.84±0.82	70.34±1.17
	Cutout	28.88±2.84	37.33±1.03	47.55±2.06	53.39±1.32	61.17±1.03	72.14±1.10
	Random Erasing	28.91±2.64	37.13±0.61	47.20±2.32	53.11±1.65	60.34±0.35	72.00±0.71
	Cosine	31.45±3.22	37.88±1.24	46.69±1.38	52.16±0.72	59.24±1.60	70.18±1.32
	MixUp	33.41±2.70	43.03±1.21	53.09±1.00	59.47±1.10	66.16±0.78	74.23±0.35
	MixUpN†	32.83±2.51	41.92±1.19	53.16±0.59	58.53±0.36	64.88±0.68	73.19±0.75
	Scattering	30.50±3.87	37.28±1.87	45.65±1.45	50.47±1.19	54.30±0.95	61.51±0.79
	GLICO	31.91±2.41	42.02±0.87	51.61±1.23	59.03±0.70	65.00±1.24	73.96±0.81
	ChimeraMix+Grid	36.94±2.63	45.57±2.11	53.67±2.84	59.66±1.35	65.42±0.83	73.76±0.30
	ChimeraMix+Seg	37.31±2.57	47.60±1.81	56.21±1.77	60.92±0.62	67.30±1.21	74.96±0.21
HydraMix	39.05±2.77	48.84±2.28	57.56±1.36	63.22±0.53	68.95±0.85	76.24±0.49	
STL-10	Baseline	27.61±0.90	31.93±1.68	36.50±0.94	39.95±1.26	44.82±0.48	53.51±1.65
	Cutout	28.05±1.73	31.45±2.46	37.68±1.30	40.69±1.13	45.63±1.19	54.32±1.01
	Random Erasing	27.87±1.36	31.32±0.48	36.91±1.45	40.66±0.84	45.93±1.10	53.31±1.52
	Cosine	25.97±0.93	30.37±1.34	35.51±0.95	40.05±1.01	45.51±1.23	53.01±1.09
	MixUp	30.06±1.80	35.63±0.85	42.44±1.85	45.00±2.71	49.03±1.34	54.38±2.11
	MixUpN†	28.93±2.54	34.45±1.04	41.31±0.63	42.17±2.09	46.21±2.27	49.57±1.15
	GLICO	26.97±0.98	33.02±1.07	37.88±1.22	42.66±0.66	48.40±0.72	54.82±1.94
	ChimeraMix+Grid	32.18±0.90	37.01±0.84	43.19±1.03	48.93±1.34	52.81±1.45	60.04±0.27
	ChimeraMix+Seg	31.37±1.72	37.05±1.09	44.74±0.60	49.58±0.49	55.06±1.11	60.44±0.71
	HydraMix	33.09±1.59	39.20±0.76	45.80±1.66	50.30±0.99	54.10±1.22	60.87±1.55
ciFAIR-100	Baseline	18.78±0.79	24.53±0.28	39.27±0.31	45.99±0.32	53.40±0.36	61.81±0.41
	Cutout	19.25±0.52	27.77±0.39	40.72±0.68	47.78±0.39	55.13±0.30	63.26±0.62
	Random Erasing	18.35±0.37	26.09±0.74	38.83±1.01	46.14±0.38	54.26±0.08	63.24±0.50
	Cosine	18.04±0.87	23.72±0.35	38.84±0.73	45.83±0.43	53.32±0.11	61.50±0.46
	MixUp	20.63±0.16	31.03±0.54	41.58±0.40	47.88±0.45	54.87±0.20	62.49±0.52
	MixUpN†	17.71±0.51	26.36±0.49	37.54±0.65	44.71±0.67	52.54±0.44	58.16±0.42
	Scattering	12.67±0.40	18.25±0.56	26.37±0.63	31.51±0.28	36.49±0.42	48.18±0.33
	GLICO	19.32±0.39	28.49±0.60	40.45±0.30	45.90±0.77	53.53±0.19	60.68±0.50
	SuperMix	19.23±0.45	26.78±0.20	38.47±0.83	44.69±0.63	53.07±0.13	62.63±0.30
	ChimeraMix+Grid	20.24±0.12	31.62±0.82	41.80±0.52	48.10±0.71	54.67±1.01	62.13±0.27
ChimeraMix+Seg	21.09±0.47	32.72±0.60	43.23±0.38	48.83±0.72	55.79±0.21	62.96±0.77	
HydraMix	24.86±0.54	33.80±0.71	44.06±0.64	49.46±0.42	56.77±0.33	63.91±0.58	

The generator and the discriminator are trained alternately. The discriminator is applied patch-wise and determines whether a patch is from a real or generated image by predicting a one or zero, respectively. The generator, on the other hand, is trained to generate images that fool the discriminator by optimizing a loss $\mathcal{L}_{G,disc}$. The loss minimizes the distance between discriminator prediction for generated images and the real label.

Finally, the total generator loss is defined as follows:

$$\mathcal{L} = \alpha_{rec}\mathcal{L}_{rec} + \alpha_{per}\mathcal{L}_{per} + \alpha_{G,disc}\mathcal{L}_{G,disc}, \quad (6)$$

where α_{rec} , α_{per} , and $\alpha_{G,disc}$ are constants (see Section 4.10).

Optionally, the generator operates on a higher image resolution by upscaling the input images \mathbf{I} by bilinear interpolation. This does not add extra information but enables the generator to produce high-frequency image details more efficiently, which is especially useful for datasets with a small image size. The generated images are downscaled to the original image size before passing them to the classifier. An analysis of the generator image size is shown in Section 4.8.3.

Table 2: Accuracy of ChimeraMix+Grid, ChimeraMix+Seg, and HydraMix with AutoAugment (AA) and TrivialAugment (TA) on ciFAIR-10, STL-10, and ciFAIR-100. The best result is highlighted in bold and the second best is underlined.

Samples per Class				5	10	30	50	100
Dataset	Method	AA	TA					
ciFAIR-10	AutoAugment	✓	–	35.64±3.23	44.43±2.19	60.80±0.75	67.18±0.99	74.86±0.40
	TrivialAugment	–	✓	31.55±3.77	41.87±1.56	58.60±1.08	66.30±0.94	75.54±0.50
	ChimeraMix+Grid	–	–	36.94±2.63	45.57±2.11	59.66±1.35	65.42±0.83	73.76±0.30
	ChimeraMix+Grid	✓	–	41.28±1.62	49.02±1.41	64.13±0.29	69.90±0.32	76.91±0.49
	ChimeraMix+Grid	–	✓	35.86±3.11	45.32±1.96	61.69±0.75	69.04±0.10	76.88±0.67
	ChimeraMix+Seg	–	–	37.31±2.57	47.60±1.81	60.92±0.62	67.30±1.21	74.96±0.21
	ChimeraMix+Seg	✓	–	42.16±1.00	49.75±1.55	65.28±0.32	70.09±0.72	76.76±0.35
	ChimeraMix+Seg	–	✓	36.74±3.55	46.58±2.15	63.21±0.48	70.24±0.85	77.79±0.46
	HydraMix	–	–	39.05±2.77	48.84±2.28	63.22±0.53	68.95±0.85	76.24±0.49
	HydraMix	✓	–	43.80 ±2.53	52.66 ±2.40	66.52 ±0.27	71.75±0.70	77.96 ±0.62
STL-10	AutoAugment	✓	–	32.05±0.93	37.65±2.26	49.77±1.09	53.84±0.96	59.55±0.96
	TrivialAugment	–	✓	30.91±1.98	35.87±1.57	47.67±0.56	53.50±1.89	61.04±0.70
	ChimeraMix+Grid	–	–	32.18±0.90	37.01±0.84	48.93±1.34	52.81±1.45	60.04±0.27
	ChimeraMix+Grid	✓	–	37.54±1.74	43.12±0.79	53.75±1.38	57.76±1.46	61.86±1.06
	ChimeraMix+Grid	–	✓	34.88±1.97	41.02±0.60	51.86±1.02	56.61±0.76	62.43±0.11
	ChimeraMix+Seg	–	–	31.37±1.72	37.05±1.09	49.58±0.49	55.06±1.11	60.44±0.71
	ChimeraMix+Seg	✓	–	36.71±1.46	43.88±0.73	54.90±1.08	56.41±2.13	60.98±0.96
	ChimeraMix+Seg	–	✓	34.53±2.01	41.08±0.44	52.03±1.80	55.66±0.72	63.83 ±0.52
	HydraMix	–	–	33.09±1.59	39.20±0.76	50.30±0.99	54.10±1.22	60.87±1.55
	HydraMix	✓	–	37.87 ±1.50	43.81±1.51	54.97 ±0.74	58.39 ±1.10	63.82±0.70
ciFAIR-100	AutoAugment	✓	–	21.39±0.95	29.56±0.68	47.58±0.56	55.01±0.24	63.69±0.42
	TrivialAugment	–	✓	23.85±0.60	32.48±0.34	50.17±0.26	56.27±0.19	64.02±0.18
	ChimeraMix+Grid	–	–	20.24±0.12	31.62±0.82	48.10±0.71	54.67±1.01	62.13±0.27
	ChimeraMix+Grid	✓	–	25.24±1.02	34.60±0.47	51.00±0.87	57.74±0.51	64.19±0.68
	ChimeraMix+Grid	–	✓	25.69±0.37	34.67±0.51	51.81±0.11	57.80±0.62	64.21±0.37
	ChimeraMix+Seg	–	–	21.09±0.47	32.72±0.60	48.83±0.72	55.79±0.21	62.96±0.77
	ChimeraMix+Seg	✓	–	25.16±0.37	35.02±0.55	51.25±0.67	57.86±0.41	64.39±0.43
	ChimeraMix+Seg	–	✓	26.36±0.17	36.02 ±0.22	52.74 ±0.20	58.90 ±0.64	64.79 ±0.06
	HydraMix	–	–	24.86±0.54	33.80±0.71	49.46±0.42	56.77±0.33	63.91±0.58
	HydraMix	✓	–	27.06 ±0.72	35.74±0.88	51.96±0.28	58.36±0.48	63.85±0.13
HydraMix	–	✓	26.21±0.58	35.23±0.89	51.45±0.44	58.11±0.62	64.33±0.26	

4. Experiments

To evaluate the performance of the proposed method, we perform several experiments that test the impact of our generated images when training a classifier, the structure of the feature space, and an extensive set of ablation and sensitivity analyses of the crucial parts of the pipeline.

We evaluate our method on three benchmark datasets that are commonly used to evaluate classification algorithms in the small data regime. The ciFAIR-10 and ciFAIR-100 datasets (Barz & Denzler, 2020b) contain 50,000 and 10,000 32×32 images in their training and test sets that are assigned to one of 10 and 100, respectively, classes. We follow the standard procedure of subsampling these images further so that they only contain a handful of samples per class for training. Additionally, we evaluate HydraMix on the STL-10 dataset (Coates et al., 2011), which offers more complex samples of size 96×96 in a 5000/8000 training and test split. This

dataset is subsampled as well, similar to the other two.

4.1. Experimental Setup

For the ciFAIR-10 and ciFAIR-100 datasets, we train a WideResNet-16-8 (Zagoruyko & Komodakis, 2016) classifier using the same hyperparameters as (Brigato et al., 2021). On STL-10, we use a ResNet-50 (He et al., 2016) due to the larger images. For all experiments, we use the same hyperparameters if not noted otherwise and optimize the networks using SGD with momentum and a cosine-annealing schedule for the learning rate. We report average metrics over five different seeds together with their standard deviation. The image segmentation is calculated in advance, such that the additional processing time is negligible.

We augment the dataset of the image classifier with generations from the trained HydraMix pipeline by injecting the samples into the classification training pipeline. Qualitative

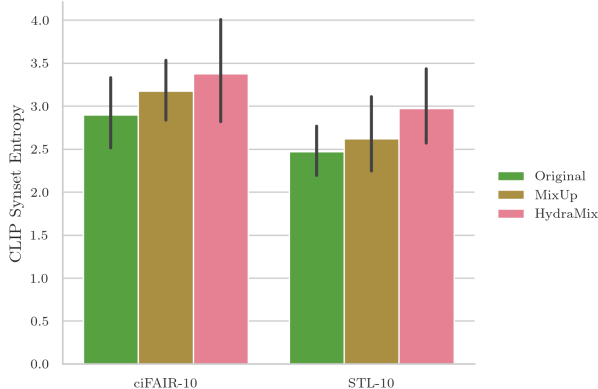


Figure 3: CLIP Synset Entropy (\uparrow) of the original dataset, a dataset generated with MixUp, and a dataset generated with HydraMix. By sampling new compositions, HydraMix is able to generate a larger variety of images that cover more synset concepts.

examples are shown in Figure 2. The results are reported for a pipeline that is trained to mix four images. We determined this hyperparameter using a grid search and report the results in Section 4.8.1. In our experiments in Section 4.8.2, we also provide a sensitivity analysis for the ratio p_{gen} between real and generated images and its effect on the final validation accuracy.

4.2. Comparison with State of the Art

Following the methodology in (Reinders et al., 2022), we evaluate HydraMix against an extensive set of state-of-the-art methods and baselines such as Cutout (DeVries & Taylor, 2017), Random Erasing (Zhong et al., 2020), Cosine loss (Barz & Denzler, 2020a), MixUp (Zhang et al., 2018), MixUp extended to multiple images denoted as MixUpN, GLICO (Azuri & Weinshall, 2021), ChimeraMix+Grid (Reinders et al., 2022), and ChimeraMix+Seg (Reinders et al., 2022). Additionally, on ciFAIR-10 and ciFAIR-100, we compare our method with the Parametric Scattering Networks (Gauthier et al., 2021) and on ciFAIR-10 we include the saliency-based method SuperMix (Dabouei et al., 2021) in our evaluation. We also evaluate a WideResNet and ResNet-50, respectively, baseline for all settings.

The results of all methods are shown in Table 1 on all datasets for different numbers of samples per class. On ciFAIR-100 with 5 images per class, for example, the baseline achieves an accuracy of 31.37%, MixUp of 33.41%, ChimeraMix+Seg of 37.31%, and HydraMix of 39.05%. On STL-10 with 10 images per class, HydraMix reaches 39.20%, outperforming ChimeraMix+Seg and MixUp, which have a test accuracy of 37.05% and 35.63%, respectively. MixUpN is an extension of MixUp to

Table 3: Comparison of different methods on ImageNet with 5 examples per class.

Method	Top-1	Top-5
Baseline	3.09	8.65
MixUp	4.40	11.31
ChimeraMix	9.44	20.76
HydraMix	9.48	21.21

Table 4: Self-supervised learning analysis: Accuracy of DINO and DINO with ChimeraMix and HydraMix on STL-10 with 5 training examples per class.

Method	
DINO	30.81 \pm 4.30
DINO+ChimeraMix	32.87 \pm 3.72
DINO+HydraMix	33.20\pm3.74

multiple images by sampling the weighting from a Dirichlet distribution. The method sometimes achieves results comparable to MixUp, but more frequently, it leads to decreased performance, often worse than the baseline, like on ciFAIR-10 and ciFAIR-100 with 5 examples per class. This shows that a straightforward mixing of multiple images is not successful.

Furthermore, we evaluate the performance of a baseline, MixUp, ChimeraMix, and HydraMix on ImageNet (Rusakovsky et al., 2015) with 5 examples per class. The Top-1 and Top-5 accuracy are shown in Table 3. While the baseline reaches 3.09%, MixUp achieves 4.40%. ChimeraMix and HydraMix significantly outperform both methods and achieve an accuracy of 9.44% and 9.48%, respectively.

Overall, the results demonstrate the superior performance of HydraMix in comparison to all other methods. Particularly in scenarios with limited data, such as 5 or 10 samples per class, the proposed method demonstrates a noticeable advantage over the prior state-of-the-art established by ChimeraMix+Seg.

4.3. Automatic Augmentation

In the next experiment, we evaluate the combination of our method with automatic augmentation techniques. While previous experiments use only basic augmentation techniques to assess the impact of the methods on the performance of the classifier, current image classification pipelines commonly use automatic augmentation policies to prevent overfitting. The results of AutoAugment (Cubuk et al., 2019), TrivialAugment (Müller & Hutter, 2021), and combinations of ChimeraMix+Grid, ChimeraMix+Seg, and HydraMix with both automatic augmentation methods are

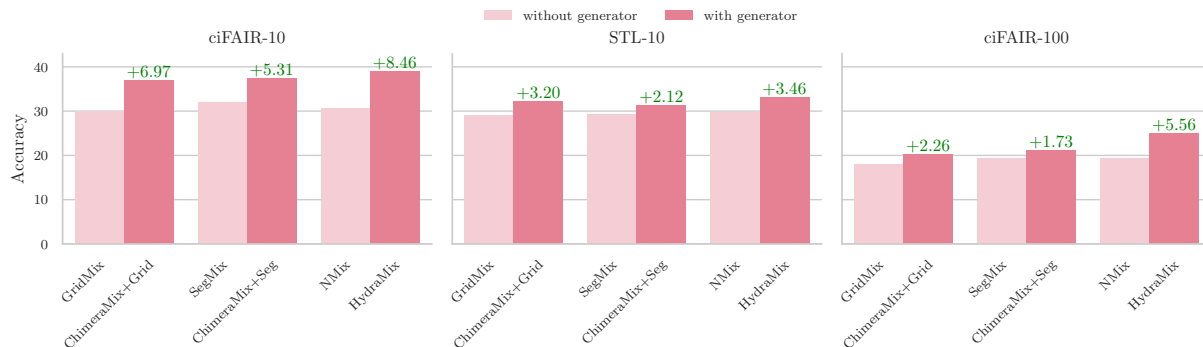


Figure 4: Average classification accuracy on the evaluated datasets with 5 samples per class of HydraMix, ChimeraMix+Grid, and HydraMix and their respective ablation methods that do not use a generator.

shown in Table 2. The experiment demonstrates that HydraMix is able to usually outperform AutoAugment and TrivialAugment, especially when few training examples are available. On ciFAIR-10 with 5 examples per class, for example, AutoAugment achieves an accuracy of 35.64% while HydraMix reaches 39.05%. The combination of HydraMix with AutoAugment boosts the performance to 43.89%. However, AutoAugment is not strictly in the small data regime as its augmentation policy was finetuned on the whole dataset.

4.4. Comparison to Self-supervised and Generative Methods

Additionally, we evaluate a self-supervised learning approach and a state-of-the-art generative method. The experiments are performed on STL-10 with 5 examples per class. DINO (Caron et al., 2021) is a widely used self-supervised learning method that leverages contrastive learning to extract meaningful representations from unlabelled data, achieving state-of-the-art performance in various tasks. We train DINO according to the original implementation and training protocol. Afterward, a linear probing is performed. The results are reported in Table 4. DINO achieves an accuracy of 30.81%. When integrating ChimeraMix and HydraMix, the performance is increased to 32.87% and 33.20%, respectively.

Next, a comparison to a state-of-the-art generative method, DiffuseMix (Islam et al., 2024), is performed. DiffuseMix generates new images with a diffusion model, more precisely a InstructPix2Pix diffusion model (Brooks et al., 2023) based on Stable Diffusion with conditional prompts. Afterward, a hybrid image is created and blended with a random fractal image. It should be noted that the model was trained on the large-scale LAION-5B dataset, comprising over 5 billion images, and is therefore not in the small data regime. The results in Table 5 show that DiffuseMix reaches 30.44%, while HydraMix outperforms it with an accuracy

Table 5: Comparison of the generative augmentation method DiffuseMix with ChimeraMix and HydraMix on STL-10 with 5 training examples per class.

Method	Accuracy
Baseline	27.61 \pm 0.90
DiffuseMix	30.44 \pm 1.19
ChimeraMix+Grid	32.18 \pm 0.90
ChimeraMix+Seg	31.37 \pm 1.72
HydraMix	33.09 \pm 1.59

of 33.09%

4.5. CLIP Synset Entropy

Analyzing the diversity of the generated data is very important. To show the generality of our approach, we employ the recently developed CLIP (Radford et al., 2021) method in combination with the Open English WordNet (Miller, 1995; McCrae et al., 2020) to measure the diversity of the generated data. CLIP consists of a shared embedding space for images and natural language, which allows the computation of the similarity between an image and a given phrase. Thus, it can act as an open-set classifier. WordNet is a lexical database consisting of words that are connected by semantic relations. Words are linked if they share the same meaning (these are called synonyms), if one is a more specific type of another (these are called hyponyms), or if they are parts of each other (known as meronyms). For example, a hyponym of `vehicle` is `car` since a car is a type of vehicle.

The classification results indicate that HydraMix generates images from a given set of examples that are more general than the original data or other augmentation methods. To further support this, we map all dataset classes to synsets s_i in the WordNet database, where $i \in [1, C]$ is the class index.

Table 6: Analysis of the generator’s impact. GridMix, SegMix, and MixN directly mix the images in pixel space without the generator of ChimeraMix or HydraMix. The study shows that mixing the features via the proposed generator (ChimeraMix+Grid, ChimeraMix+Seg, and HydraMix) is able to learn the generation of new image compositions and achieves a significantly improved performance.

Samples per Class		5	10	20	30	50	100
Dataset	Method						
ciFAIR-10	GridMix	29.97±1.17	39.90±1.24	48.60±3.18	54.99±2.49	61.12±1.59	72.41±0.69
	SegMix	32.00±1.22	42.18±1.36	52.56±2.43	57.90±0.49	64.61±0.94	73.96±0.36
	NMix	30.59±4.04	40.69±1.25	50.63±2.04	56.25±1.51	64.03±0.93	73.51±0.92
	ChimeraMix+Grid	36.94±2.63	45.57±2.11	53.67±2.84	59.66±1.35	65.42±0.83	73.76±0.30
	ChimeraMix+Seg	37.31±2.57	47.60±1.81	56.21±1.77	60.92±0.62	67.30±1.21	74.96±0.21
	HydraMix	39.05±2.77	48.84±2.28	57.56±1.36	63.22±0.53	68.95±0.85	76.24±0.49
STL-10	GridMix	28.98±1.49	31.21±1.52	37.08±1.09	42.14±1.52	49.33±0.88	56.92±0.51
	SegMix	29.25±0.40	32.84±0.63	37.80±1.91	43.69±0.84	50.14±0.84	58.60±0.57
	NMix	29.63±1.04	33.85±2.15	40.35±0.97	44.72±1.11	50.11±1.66	59.32±0.81
	ChimeraMix+Grid	32.18±0.90	37.01±0.84	43.19±1.03	48.93±1.34	52.81±1.45	60.04±0.27
	ChimeraMix+Seg	31.37±1.72	37.05±1.09	44.74±0.60	49.58±0.49	55.06±1.11	60.44±0.71
	HydraMix	33.09±1.59	39.20±0.76	45.80±1.66	50.30±0.99	54.10±1.22	60.87±1.55
ciFAIR-100	GridMix	17.98±0.23	27.78±0.46	38.92±0.05	45.16±1.05	52.97±0.30	61.37±0.26
	SegMix	19.36±0.82	29.62±0.22	41.00±0.42	47.50±0.38	54.62±0.15	62.43±0.38
	NMix	19.30±0.31	29.30±0.71	39.90±0.53	46.26±0.30	54.13±0.32	62.85±0.54
	ChimeraMix+Grid	20.24±0.12	31.62±0.82	41.80±0.52	48.10±0.71	54.67±1.01	62.13±0.27
	ChimeraMix+Seg	21.09±0.47	32.72±0.60	43.23±0.38	48.83±0.72	55.79±0.21	62.96±0.77
	HydraMix	24.86±0.54	33.80±0.71	44.06±0.64	49.46±0.42	56.77±0.33	63.91±0.58

For each synset, we extract all subordinate synsets that are hyponyms of s_i denoted as $H_i = \{h_{i,1}, \dots, h_{i,N_i}\}$ and N_i is the number of hyponyms. For example, the class Dog has the hyponyms puppy, police dog, and Chihuahua and Truck has the hyponyms fire truck, tow car, and dump truck, among others. The features of the generated images should cover more subclasses of a given class.

We use a CLIP image encoder $f_{\text{Image}}^{\text{CLIP}}(\mathbf{x})$ and text encoder $f_{\text{Text}}^{\text{CLIP}}(t)$ based on a ViT-B/16 architecture (Dosovitskiy et al., 2021) pretrained on LAION-2B (Schuhmann et al., 2022) using OpenCLIP (Ilharco et al., 2021). To encode synsets, we introduce a Synset-to-Text function $f_{\text{S2T}}(s)$ that generates a textual representation of a synset by combining all K synonyms and the description of a synset in the format “*Synonym₁, ..., Synonym_K : Description*”. The similarity $\text{sim}(\mathbf{x}, s)$ between an image x and a synset s is defined as the cosine similarity of the encoded image and the encoded synset:

$$\text{sim}(\mathbf{x}, s) = \frac{f_{\text{Image}}^{\text{CLIP}}(\mathbf{x}) \cdot f_{\text{Text}}^{\text{CLIP}}(f_{\text{S2T}}(s))}{\|f_{\text{Image}}^{\text{CLIP}}(\mathbf{x})\| \cdot \|f_{\text{Text}}^{\text{CLIP}}(f_{\text{S2T}}(s))\|}. \quad (7)$$

We compute the CLIP embeddings of the original images, the images produced by the MixUp method, and our generated images. For MixUp and HydraMix, we sample 1000 images per class. Then, the synsets $h_{i,j}$ are encoded, and similarities between all images and synsets are calculated. For each dataset, we calculate the synset distribution per class $P(h_{i,j})$ by averaging the synset distribution for

each image, which is determined as the softmax across all synsets:

$$P(h_{i,j}) = \frac{1}{N} \sum_{l=1}^N \frac{\exp(\text{sim}(\mathbf{x}_l, h_{i,j})/\tau)}{\sum_{k=1}^{N_i} \exp(\text{sim}(\mathbf{x}_l, h_{i,k})/\tau)}, \quad (8)$$

where τ is a temperature parameter and N the number of images per class.

Finally, we measure the diversity of the dataset per class by computing the entropy of the synset distribution:

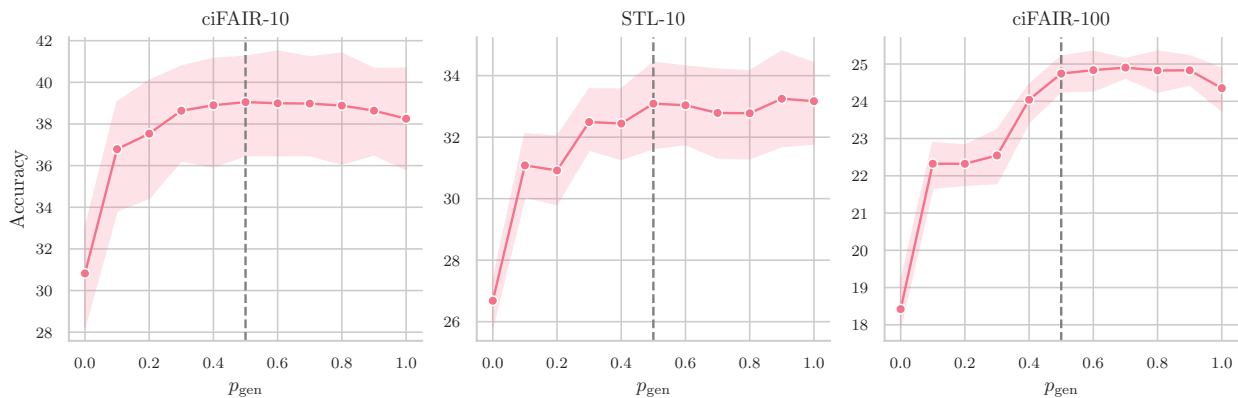
$$\text{CSE}_i = - \sum_{j=1}^{N_i} P(h_{i,j}) \log(P(h_{i,j})). \quad (9)$$

The CLIP Synset Entropy CSE_i measures the hyponym coverage of a set of images for each class. We compute the overall CLIP Synset Entropy across all classes as CSE by averaging CSE_i .

The results, shown in Figure 3, support the outcome of our classification experiments. The features of the images that are generated by HydraMix are more similar to a larger range of synset concepts. On both datasets, HydraMix enables the generation of a more diverse range of images, which enhances the average synset similarity distribution. On STL-10, the original dataset has a CSE of 2.47. MixUp achieves 2.61 and HydraMix reaches 2.97.

Table 7: Analysis of the number of mixing images for HydraMix.

Samples per Class		5	10	20	30	50	100
Dataset	#Mixing Images						
ciFAIR-10	2	38.02 \pm 3.08	48.76 \pm 1.79	56.90 \pm 1.69	62.94 \pm 0.77	68.67 \pm 0.84	75.81 \pm 0.48
	3	38.48 \pm 3.08	48.47 \pm 2.11	57.98 \pm 1.45	62.97 \pm 0.89	69.12 \pm 1.06	76.00 \pm 0.48
	4	39.05 \pm 2.77	48.84 \pm 2.28	57.56 \pm 1.36	63.22 \pm 0.53	68.95 \pm 0.85	76.24 \pm 0.49
	5	37.84 \pm 3.43	48.19 \pm 1.73	57.75 \pm 1.98	63.39 \pm 0.78	68.85 \pm 0.65	75.92 \pm 0.41
STL-10	2	32.32 \pm 1.69	38.57 \pm 1.62	44.76 \pm 1.44	49.28 \pm 1.50	54.31 \pm 0.85	61.24 \pm 1.12
	3	32.90 \pm 2.15	38.36 \pm 1.38	44.83 \pm 0.24	49.75 \pm 1.07	54.62 \pm 0.47	60.99 \pm 1.25
	4	33.09 \pm 1.59	39.20 \pm 0.76	45.80 \pm 1.66	50.30 \pm 0.99	54.10 \pm 1.22	60.87 \pm 1.55
	5	32.57 \pm 1.92	39.28 \pm 1.57	46.10 \pm 0.66	50.66 \pm 0.71	55.48 \pm 0.78	62.36 \pm 0.94
ciFAIR-100	2	23.50 \pm 0.45	33.84 \pm 0.64	44.02 \pm 0.58	50.03 \pm 0.66	56.95 \pm 0.33	64.24 \pm 0.26
	3	24.66 \pm 0.77	34.03 \pm 0.77	44.51 \pm 0.77	50.15 \pm 0.76	56.62 \pm 0.44	64.41 \pm 0.23
	4	24.86 \pm 0.54	33.80 \pm 0.71	44.06 \pm 0.64	49.46 \pm 0.42	56.77 \pm 0.33	63.91 \pm 0.58
	5	24.58 \pm 0.85	33.82 \pm 0.41	43.88 \pm 0.69	49.62 \pm 0.45	56.48 \pm 0.47	63.88 \pm 0.31

Figure 5: Evaluation of the mixing probability p_{gen} on different datasets. The default mixing ratio of 0.5 is indicated by a dashed line. Experiments are performed with 5 examples per class.

4.6. Generator Impact

We investigate the impact of the proposed generator on the generated samples. For this, we evaluate each method (ChimeraMix+Grid, ChimeraMix+Seg, and HydraMix) against a baseline that performs the mixing in pixel space without the use of the generator. The pixel-based methods will be denoted as GridMix, SegMix, and NMix. The average accuracy of all methods is shown in Figure 4 with 5 examples per class. The results demonstrate a noticeable improvement for all methods that employ a generator on all datasets, highlighting the importance of the generator. The most significant improvement is apparent for HydraMix. On ciFAIR-100, for example, the performance without the generator (NMix) is 30.59%, while the performance with the generator is 39.05% (+8.46 percentage points).

The results in Figure 4 demonstrate the advantage of the proposed generator and its operation in the mixed feature space. We report detailed performance metrics for varying numbers of samples per class in Table 6. It is apparent that our

pipeline is especially useful in the small data regime with 20 samples or less per class, but also increases performance with more samples.

4.7. Object Detection

Furthermore, we extend HydraMix to object detection tasks as a proof-of-concept, demonstrating its applicability beyond classification. Using Faster R-CNN (Ren et al., 2015), we evaluate the method on the COCO dataset (Lin et al., 2014). For training, we subsample the dataset by randomly selecting N images for each class, denoted as N -shot. HydraMix leverages the bounding box information to generate mixing masks. The results, presented in Table 8, highlight the potential of HydraMix in enhancing performance in complex vision tasks. On 1-shot and 3-shot, HydraMix boosts the performance by 28.9% and 19.8%, respectively. This approach also opens up significant opportunities for further extensions, particularly by incorporating semantic information.

Table 8: Object detection performance on COCO with very few training samples using Faster R-CNN when integrating HydraMix as a proof-of-concept.

Shot	Method	AP	AP ₅₀	AP ₇₅
1	Baseline	1.27 \pm 0.06	2.90 \pm 0.20	1.00 \pm 0.00
	Baseline + HydraMix	1.63 \pm 0.15(+28.9%)	3.73 \pm 0.32(+28.7%)	1.23 \pm 0.12(+23.3%)
3	Baseline	3.37 \pm 0.06	7.20 \pm 0.20	2.83 \pm 0.15
	Baseline + HydraMix	4.03 \pm 0.21(+19.8%)	8.53 \pm 0.31(+18.5%)	3.40 \pm 0.30(+20.0%)

4.8. Analyses

In the following, we perform several analyses to examine the robustness of the individual components as well as the parameters of the proposed method.

4.8.1. MIXING MULTIPLE IMAGES

The presented method enables mixing more than two images, which exponentially expands the space of combinations. In the next experiment, we analyze the influence of mixing multiple images. There is a trade-off between the number of segments in each image, which is heavily influenced by the image size, and the noise that mixing more than two images introduces into the data samples. Thus, the optimal number of images varies and depends on the number of samples per class and the image size. We perform a grid search over the number of mixed images between two and five for all datasets and evaluate the downstream classification performance. The results in Table 7 demonstrate that mixing multiple images is very effective. The optimal number of images indeed varies depending on the dataset. In the case of STL-10, the optimal performance is attained by mixing a larger quantity of images, specifically five images. For ciFAIR-100, the best results are achieved by combining three images. Overall, mixing four images consistently yields strong performance across all configurations of this hyperparameter.

4.8.2. MIXING RATIO

The amount of the generated images is controlled by the mixing probability p_{gen} . At each training step of the classifier, we sample with p_{gen} whether generating new images or training on a batch of original images. A larger p_{gen} results in a more extensive augmented dataset because the classifier is trained on more generated samples. It controls the trade-off between data variability and the similarity of the training data distribution to the original small dataset. In Figure 5, we show the results of training a large number of classifiers with different mixing ratios in the setting with 5 samples per class and report the average validation accuracy. When the mixing ratio is set to zero, we only train with the original images. When $p_{\text{gen}} = 1$, the classifier is trained

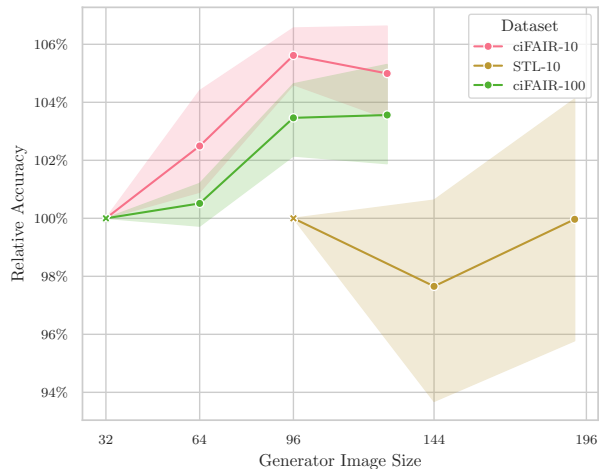


Figure 6: Analysis of the generator image size for different datasets showing the relative accuracy compared to the performance with the original image size (indicated by cross). On datasets with a small image size, such as ciFAIR-10 and ciFAIR-100, lifting the generator to a large image size achieves a performance gain. Experiments are performed with 5 examples per class. The downstream classifier is always trained on the original image size.

with generated images exclusively. This experiment shows that integrating a large portion of generated images (i.e., a mixing ratio between 40% and 90%) is very effective. The optimal mixing ratio varies slightly between the datasets but is generally reasonably robust. Replacing every second image in the classifier pipeline with a generated mix is a good choice across all datasets.

4.8.3. GENERATOR IMAGE SIZE

In the next analysis, we investigate operating the generator on a larger image resolution as proposed in Section 3.5. For that, the input images are upsampled by bilinear interpolation to a target image size before processing by the generator. Afterward, the output of the generator is downsampled to the original image size accordingly. In this process, no additional information is required, and the generator is enabled

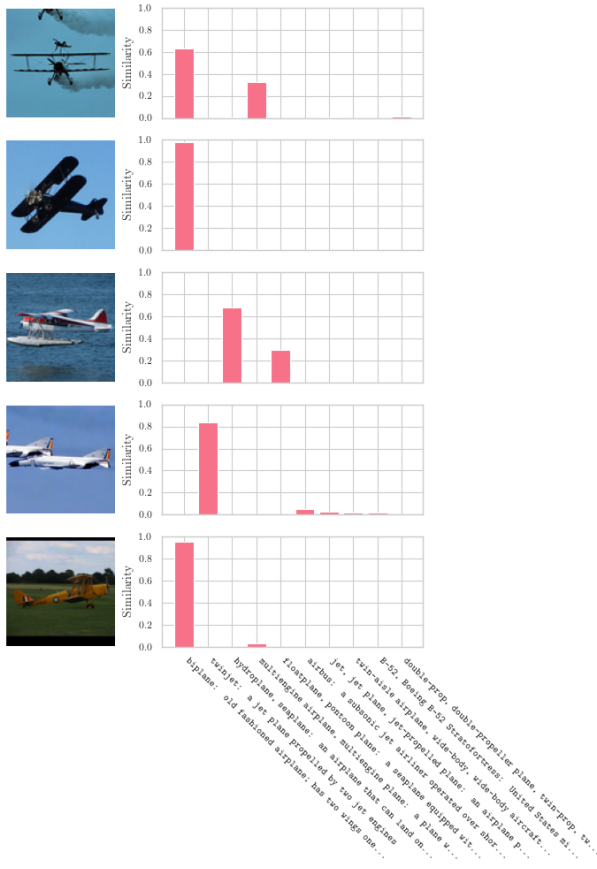


Figure 7: Distribution of the synset similarity with respect to each image. Images from the class Airplane of the STL-10 dataset and the top 10 synsets sorted by average similarity are shown. The synsets are represented by the format “ $Synonym_1, \dots, Synonym_K: Description$ ”. The similarities are computed using the CLIP embeddings of the synset representations and the images.

to more effortlessly produce high-frequency details, especially for datasets with a small image size. The classifier is always trained on the original image size.

The relative classification accuracy compared to the classification accuracy on the original image size with different generator image sizes is shown in Figure 6. The results show that for datasets with a small image size (ciFAIR-10 and ciFAIR-100), operating the generator on a larger image size is very effective. A generator image size of 96×96 , for example, boosts the performance by 5.61% on ciFAIR-10 and 3.46% on ciFAIR-100. On STL-10, which has larger images, increasing the generator image size to 1.5x of the original image size leads to a slightly decreased performance, while increasing the generator image size by 2x achieves the same performance. Thus, operating the generator on a larger image resolution is not necessary for datasets with an already

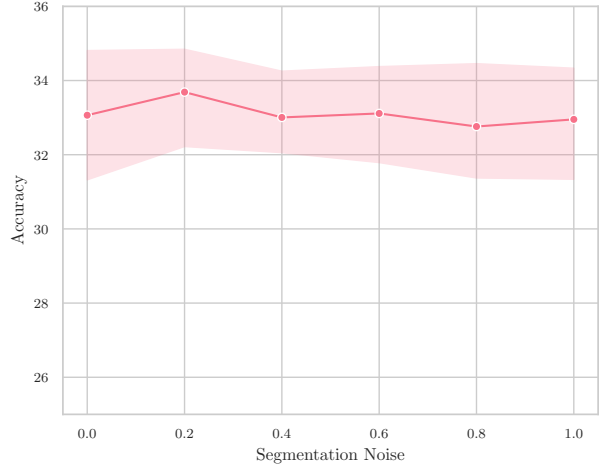


Figure 8: Analysis of the impact of noisy segmentation masks on HydraMix on STL-10 with 5 examples per class.

large image size.

4.8.4. INFLUENCE OF NOISY SEGMENTATION MASKS

In the following analysis, we evaluate the influence of noisy segmentation masks. ChimeraMix+Seg and HydraMix sample mixing masks based on the segmentation masks. A Felzenszwalb Segmentation algorithm is employed here, whereas any segmentation algorithm can be integrated. To analyze the impact of noisy segmentation masks, the masks are synthetically distorted by introducing a segmentation noise factor. With this probability, each segment is replaced with the segmentation from a different image, which is randomly selected. Thus, the segmentation noise factor serves as a parameter, varying from the original segmentation (Segmentation Noise = 0) to a completely incorrect segmentation from a different image (Segmentation Noise = 1). The results of HydraMix on STL-10 with 5 examples per class are shown in Figure 8. It can be seen that HydraMix is very robust to noisy segmentation masks.

4.8.5. CROSS-DOMAIN ANALYSIS

In a final analysis, the cross-domain generalization of HydraMix is evaluated by training a generator on one domain and performing the downstream classification on another domains. The results are shown in Table 9. In each row, a generator is trained on the respective dataset. Subsequently, the generators are integrated into the training of the downstream classifier across different datasets, as shown in the respective columns. Interestingly, on STL-10, the performance improves from 33.09% to 34.20% and 35.72% when integrated the generator trained on ciFAIR-10 and ciFAIR-100, respectively. While ciFAIR-10 has the same number of training samples, ciFAIR-100 has ten times as many

Table 9: Cross-domain analysis of HydraMix. The generator is trained on one dataset (per row) and integrated into the training of the downstream classifier on different datasets (per column).

		Downstream Classifier Dataset			Average
		ciFAIR-10	STL-10	ciFAIR-100	
Generator Dataset	ciFAIR-10	39.05 \pm 2.77	34.20 \pm 1.80	21.81 \pm 1.53	31.69 \pm 2.03
	STL-10	36.42 \pm 3.11	33.09 \pm 1.59	20.93 \pm 1.27	30.15 \pm 1.99
	ciFAIR-100	37.39 \pm 3.02	35.72 \pm 1.73	24.86 \pm 0.54	32.66 \pm 1.76

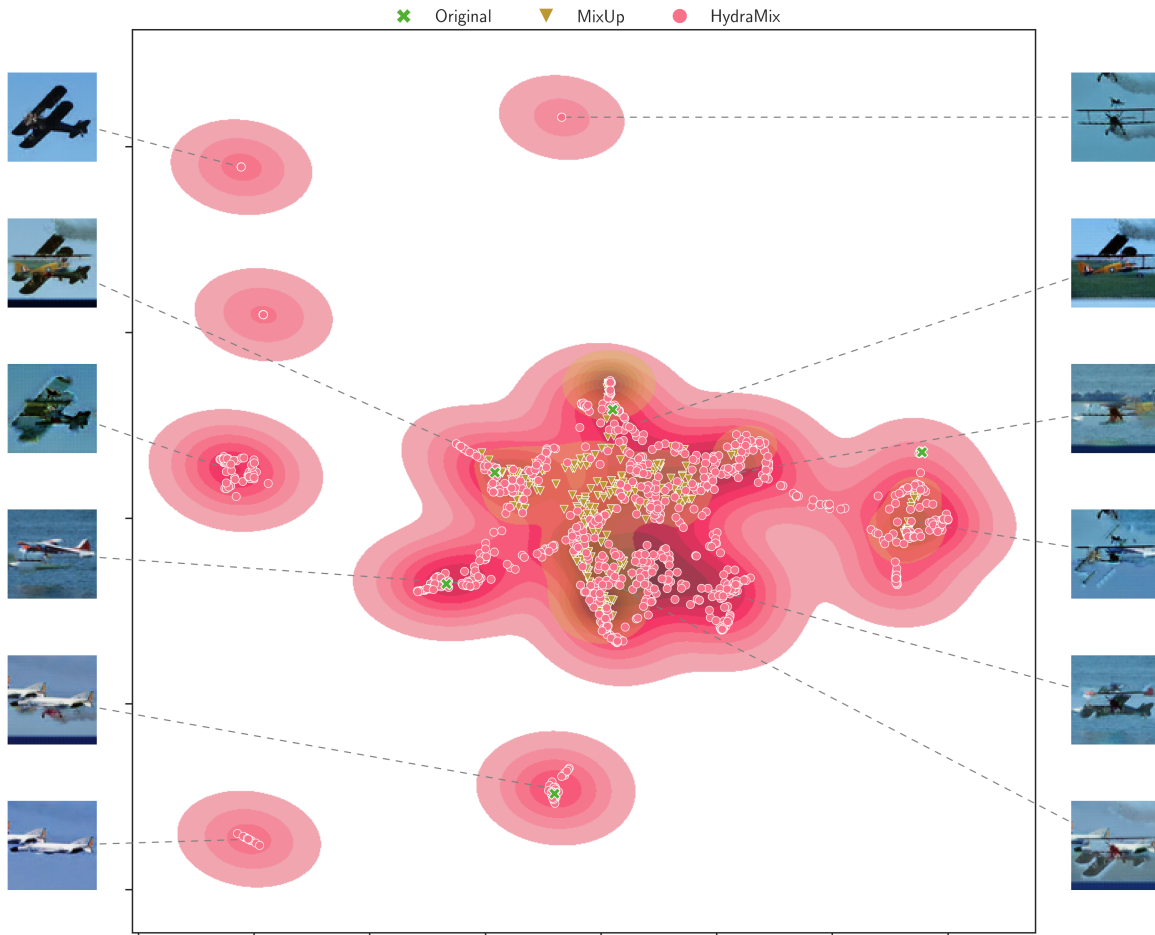


Figure 9: Visualization of the image embeddings with CLIP. The original images (green cross), MixUp images (yellow triangles), and HydraMix images (red dots). The density distribution of MixUp is highlighted in yellow, and the density distribution of HydraMix is highlighted in red.

training samples due to its larger number of classes. On ciFAIR-10 and ciFAIR-100, the best results is achieved when the generator is trained on the same dataset. Overall, the results demonstrate that HydraMix can successfully generalize across different data distributions while maintaining competitive performance. In the last column, the average downstream classifier accuracy across different datasets for each generator is shown.

4.9. CLIP Features

To assess the generalization capabilities of the mixed generated images, we introduce the novel CLIP Synset Entropy metric CSE in Section 4.5. The metric is computed as the entropy of the average similarity distribution between a set of images and all hyponyms of the synset of the class. The textual representations of a synset consist of its synonyms as well as the description. In Figure 7, we show an example of

Table 10: Common hyperparameters of the HydraMix generator for all datasets.

Epochs	200
Optimizer	Adam, $\beta=[0.5, 0.999]$
Learning Rate Schedule	Stepwise Decay of 0.2@[60,120,160]
Initial Learning Rate	0.0002
Weight Decay	0.0005
Residual Blocks	4
Feature Mixing after Block	2
Mixing Mask Size	4

the similarity distributions between a set of original images of the class `Airplane` and the synset representations. It is evident that by measuring the similarity to the hyponyms of each class, we can identify sub-concepts within a class, such as `biplane`, `twinjet`, or `hydroplane`. Therefore, the CLIP Synset Entropy serves as an effective metric for assessing the diversity within a generated dataset by calculating the coverage of the hyponyms.

To further highlight the structure of the generated images by HydraMix, we visualize the CLIP embedding space of the original subsampled dataset, the embeddings of MixUp images, and the HydraMix combinations using PaCMAP (Wang et al., 2021). An example of the class `Airplane` on STL-10 with 5 samples per class is shown in Figure 9. The original images are marked with a green cross. For MixUp and HydraMix, the image embeddings as well as the density distributions are shown in yellow and red, respectively. The embedding demonstrates that HydraMix is able to cover a much larger portion of the space between the original samples compared to MixUp.

4.10. Hyperparameters of HydraMix

The loss terms in Equation (6) are defined as $\alpha_{\text{rec}} = 1000$, $\alpha_{\text{per}} = 1$, and $\alpha_{\text{G,disc}} = 1$ to balance the small magnitude of the mean squared error reconstruction loss. In Section 4.5, we set the softmax temperature parameter τ to 1/100 to sharpen the similarity distributions. Further hyperparameters of HydraMix are shown in Table 10.

5. Conclusion

In this work, we presented a novel method for generating new image compositions from only a handful of images that achieves state-of-the-art results in small data image classification. The architecture introduces a feature-mixing architecture that combines the content from an arbitrary number of images guided by a segmentation-based mixing mask. Extensive experiments demonstrated the superior performance of HydraMix compared to existing approaches in

the small data regime. Additionally, HydraMix can be successfully combined with automated augmentation methods. Finally, we presented a CLIP Synset Entropy to analyze the distribution of the generated images and showed that HydraMix is able to generate a larger variety of synset concepts. In the future, we would like to explore unsupervised segmentation methods like (Engelcke et al., 2021) that are trained end-to-end with the generator to cluster the latent features and adjust them for the small data regime.

Acknowledgements

This work was supported by the Federal Ministry of Education and Research (BMBF), Germany under the AI service center KISSKI (grant no. 01IS22093C) and the Deutsche Forschungsgemeinschaft (DFG) under Germany’s Excellence Strategy within the Cluster of Excellence PhoenixD (EXC 2122).

References

- Arora, S., Du, S. S., Li, Z., Salakhutdinov, R., Wang, R., and Yu, D. Harnessing the power of infinitely wide deep nets on small-data tasks. In *Proc. of ICLR*, 2020.
- Azuri, I. and Weinsshall, D. Generative latent implicit conditional optimization when learning from small sample. In *25th International Conference on Pattern Recognition, ICPR*, pp. 8584–8591, 2021. doi: 10/gn3cdn.
- Barz, B. and Denzler, J. Deep Learning on Small Datasets without Pre-Training using Cosine Loss. In *IEEE Winter Conference on Applications of Computer Vision, WACV, 2020a*. ISBN 978-1-72816-553-0. doi: 10/gm84cd.
- Barz, B. and Denzler, J. Do we train on test data? Purging CIFAR of near-duplicates. *Journal of Imaging*, 6, 2020b. doi: 10/gjqb98.
- Bommasani, R., Hudson, D. A., Adeli, E., Altman, R., Arora, S., von Arx, S., Bernstein, M. S., Bohg, J., Bosselut, A., Brunskill, E., Brynjolfsson, E., Buch, S., Card, D., Castellon, R., Chatterji, N., Chen, A., Creel, K., Davis, J. Q., Demszky, D., Donahue, C., Doumbouya, M., Durmus, E., Ermon, S., Etchemendy, J., Ethayarajh, K., Fei-Fei, L., Finn, C., Gale, T., Gillespie, L., Goel, K., Goodman, N., Grossman, S., Guha, N., Hashimoto, T., Henderson, P., Hewitt, J., Ho, D. E., Hong, J., Hsu, K., Huang, J., Icard, T., Jain, S., Jurafsky, D., Kalluri, P., Karamcheti, S., Keeling, G., Khani, F., Khattab, O., Koh, P. W., Krass, M., Krishna, R., Kuditipudi, R., Kumar, A., Ladhak, F., Lee, M., Lee, T., Leskovec, J., Levent, I., Li, X. L., Li, X., Ma, T., Malik, A., Manning, C. D., Mirchandani, S., Mitchell, E., Munyikwa, Z., Nair, S., Narayan, A., Narayanan, D., Newman, B., Nie, A., Niebles, J. C.,

- Nilforoshan, H., Nyarko, J., Ogut, G., Orr, L., Papadimitriou, I., Park, J. S., Piech, C., Portelance, E., Potts, C., Raghunathan, A., Reich, R., Ren, H., Rong, F., Roohani, Y., Ruiz, C., Ryan, J., Ré, C., Sadigh, D., Sagawa, S., Sathianam, K., Shih, A., Srinivasan, K., Tamkin, A., Taori, R., Thomas, A. W., Tramèr, F., Wang, R. E., Wang, W., Wu, B., Wu, J., Wu, Y., Xie, S. M., Yasunaga, M., You, J., Zaharia, M., Zhang, M., Zhang, T., Zhang, X., Zhang, Y., Zheng, L., Zhou, K., and Liang, P. On the opportunities and risks of foundation models, 2021.
- Bornschein, J., Visin, F., and Osindero, S. Small data, big decisions: Model selection in the small-data regime. In *Proc. of ICML*, 2020.
- Breiman, L. Random Forests. *Machine Learning*, 45(1): 5–32, October 2001. ISSN 1573-0565. doi: 10.1023/A:1010933404324.
- Brigato, L. and Iocchi, L. A close look at deep learning with small data. *25th International Conference on Pattern Recognition, ICPR*, pp. 2490–2497, 2021. doi: 10/gn3cds.
- Brigato, L., Barz, B., Iocchi, L., and Denzler, J. Tune it or don’t use it: Benchmarking data-efficient image classification. *IEEE/CVF International Conference on Computer Vision Workshops, ICCVW*, pp. 1071–1080, 2021. doi: 10/gn3cfv.
- Brooks, T., Holynski, A., and Efros, A. A. Instructpix2pix: Learning to follow image editing instructions. In *Proceedings of the IEEE/CVF Conference on Computer Vision and Pattern Recognition*, pp. 18392–18402, 2023.
- Caron, M., Touvron, H., Misra, I., Jégou, H., Mairal, J., Bojanowski, P., and Joulin, A. Emerging Properties in Self-Supervised Vision Transformers. In *Proceedings of the International Conference on Computer Vision (ICCV)*, 2021.
- Coates, A., Ng, A., and Lee, H. An analysis of single-layer networks in unsupervised feature learning. In *Proceedings of the Fourteenth International Conference on Artificial Intelligence and Statistics*, volume 15 of *Proceedings of Machine Learning Research*, pp. 215–223. PMLR, 2011.
- Cubuk, E. D., Zoph, B., Mané, D., Vasudevan, V., and Le, Q. V. AutoAugment: Learning augmentation strategies from data. In *IEEE Conference on Computer Vision and Pattern Recognition, CVPR*, pp. 113–123, 2019. doi: 10/ggvxs4.
- Dabouei, A., Soleymani, S., Taherkhani, F., and Nasrabadi, N. M. SuperMix: Supervising the mixing data augmentation. *IEEE/CVF Conference on Computer Vision and Pattern Recognition, CVPR*, pp. 13789–13798, 2021. doi: 10/gnqj42.
- Denton, E. L., Chintala, S., Szlam, A., and Fergus, R. Deep generative image models using a laplacian pyramid of adversarial networks. In Cortes, C., Lawrence, N. D., Lee, D. D., Sugiyama, M., and Garnett, R. (eds.), *Advances in Neural Information Processing Systems 28*, pp. 1486–1494, 2015.
- DeVries, T. and Taylor, G. W. Improved Regularization of Convolutional Neural Networks with Cutout. *ArXiv preprint*, abs/1708.04552, 2017.
- Dosovitskiy, A., Beyer, L., Kolesnikov, A., Weissenborn, D., Zhai, X., Unterthiner, T., Dehghani, M., Minderer, M., Heigold, G., Gelly, S., Uszkoreit, J., and Houshy, N. An Image is Worth 16x16 Words: Transformers for Image Recognition at Scale. In *ICLR*, pp. 21, 2021.
- Engelcke, M., Jones, O. P., and Posner, I. GENESIS-V2: Inferring Unordered Object Representations without Iterative Refinement. In *Neural Information Processing Systems*, 2021.
- Felzenszwalb, P. F. and Huttenlocher, D. P. Efficient Graph-Based Image Segmentation. *International Journal of Computer Vision*, 59(2), 2004. ISSN 0920-5691. doi: 10/fdmw8q.
- Gauthier, S., Thérien, B., Alsène-Racicot, L., Rish, I., Belilovsky, E., Eickenberg, M., and Wolf, G. Parametric Scattering Networks. *ArXiv preprint*, abs/2107.09539, 2021.
- He, K., Zhang, X., Ren, S., and Sun, J. Deep Residual Learning for Image Recognition. In *2016 IEEE Conference on Computer Vision and Pattern Recognition (CVPR)*, pp. 770–778, Las Vegas, NV, USA, June 2016. IEEE. ISBN 978-1-4673-8851-1. doi: 10.1109/CVPR.2016.90.
- Henderson, P., Li, X., Jurafsky, D., Hashimoto, T., Lemley, M. A., and Liang, P. Foundation Models and Fair Use, March 2023.
- Ilharco, G., Wortsman, M., Wightman, R., Gordon, C., Carlini, N., Taori, R., Dave, A., Shankar, V., Namkoong, H., Miller, J., Hajishirzi, H., Farhadi, A., and Schmidt, L. OpenCLIP. Zenodo, July 2021.
- Islam, K., Zaheer, M. Z., Mahmood, A., and Nandakumar, K. DiffuseMix: Label-preserving data augmentation with diffusion models. In *Proceedings of the IEEE/CVF Conference on Computer Vision and Pattern Recognition*, pp. 27621–27630, 2024.
- Jeong, J., Park, S., Kim, M., Lee, H.-C., Kim, D., and Shin, J. SmoothMix: Training Confidence-calibrated Smoothed

- Classifiers for Certified Robustness. In *Advances in Neural Information Processing Systems*, November 2021.
- Kang, M. and Kim, S. GuidedMixup: An Efficient Mixup Strategy Guided by Saliency Maps. *Proceedings of the AAAI Conference on Artificial Intelligence*, 37(1):1096–1104, June 2023. ISSN 2374-3468, 2159-5399. doi: 10.1609/aaai.v37i1.25191.
- Kim, J.-H., Choo, W., and Song, H. O. Puzzle Mix: Exploiting Saliency and Local Statistics for Optimal Mixup. In *International Conference on Machine Learning (ICML)*, December 2020.
- Krizhevsky, A., Sutskever, I., and Hinton, G. E. ImageNet classification with deep convolutional neural networks. In Bartlett, P. L., Pereira, F. C. N., Burges, C. J. C., Bottou, L., and Weinberger, K. Q. (eds.), *Advances in Neural Information Processing Systems 25*, pp. 1106–1114, 2012.
- Li, S., Wang, Z., Liu, Z., Wu, D., Tan, C., Jin, W., and Li, S. Z. OpenMixup: A Comprehensive Mixup Benchmark for Visual Classification, October 2023.
- Liang, W., Liang, Y., and Jia, J. MiAMix: Enhancing Image Classification through a Multi-stage Augmented Mixed Sample Data Augmentation Method. *Processes*, 11(12), August 2023.
- Lin, T.-Y., Maire, M., Belongie, S. J., Hays, J., Perona, P., Ramanan, D., Dollár, P., and Zitnick, C. L. Microsoft COCO: Common objects in context. In *European Conference on Computer Vision*, 2014.
- McCrae, J. P., Rademaker, A., Rudnicka, E., and Bond, F. English WordNet 2020: Improving and extending a WordNet for English using an open-source methodology. In Declerk, T., Gonzalez-Dios, I., and Rigau, G. (eds.), *Proceedings of the LREC 2020 Workshop on Multimodal Wordnets (MMW2020)*, pp. 14–19, Marseille, France, May 2020. The European Language Resources Association (ELRA). ISBN 979-10-95546-41-2.
- Miller, G. A. WordNet: A lexical database for English. *Communications of the ACM*, 38(11):39–41, November 1995. ISSN 0001-0782, 1557-7317. doi: 10.1145/219717.219748.
- Müller, S. and Hutter, F. TrivialAugment: Tuning-free yet state-of-the-art data augmentation. In *IEEE/CVF International Conference on Computer Vision (ICCV)*, 2021.
- Neyshabur, B., Sedghi, H., and Zhang, C. What is being transferred in transfer learning? In Larochelle, H., Ranzato, M., Hadsell, R., Balcan, M. F., and Lin, H. (eds.), *Advances in Neural Information Processing Systems 33*, pp. 512–523, 2020.
- Radford, A., Kim, J. W., Hallacy, C., Ramesh, A., Goh, G., Agarwal, S., Sastry, G., Askell, A., Mishkin, P., Clark, J., Krueger, G., and Sutskever, I. Learning Transferable Visual Models From Natural Language Supervision. In *Proceedings of the 38th International Conference on Machine Learning*, Proceedings of Machine Learning Research, February 2021.
- Reinders, C., Ackermann, H., Yang, M. Y., and Rosenhahn, B. Object Recognition from very few Training Examples for Enhancing Bicycle Maps. In *2018 IEEE Intelligent Vehicles Symposium (IV)*, May 2018.
- Reinders, C., Schubert, F., and Rosenhahn, B. ChimeraMix: Image classification on small datasets via masked feature mixing. In *31st International Joint Conference on Artificial Intelligence and the 25th European Conference on Artificial Intelligence (IJCAI-ECAI)*, 2022.
- Ren, S., He, K., Girshick, R., and Sun, J. Faster R-CNN: Towards real-time object detection with region proposal networks. In Cortes, C., Lawrence, N., Lee, D., Sugiyama, M., and Garnett, R. (eds.), *Advances in Neural Information Processing Systems*, volume 28. Curran Associates, Inc., 2015.
- Rombach, R., Blattmann, A., Lorenz, D., Esser, P., and Ommer, B. High-Resolution Image Synthesis with Latent Diffusion Models. In *Proceedings of the IEEE/CVF Conference on Computer Vision and Pattern Recognition*, April 2022.
- Russakovsky, O., Deng, J., Su, H., Krause, J., Satheesh, S., Ma, S., Huang, Z., Karpathy, A., Khosla, A., Bernstein, M., Berg, A. C., and Fei-Fei, L. ImageNet Large Scale Visual Recognition Challenge. *International Journal of Computer Vision*, 115(3), 2015. ISSN 0920-5691, 1573-1405. doi: 10/gcggk7w.
- Schuhmann, C., Beaumont, R., Vencu, R., Gordon, C., Wightman, R., Cherti, M., Coombes, T., Katta, A., Mullis, C., Wortsman, M., Schramowski, P., Kundurthy, S., Crowson, K., Schmidt, L., Kaczmarczyk, R., and Jitsev, J. LAION-5B: An open large-scale dataset for training next generation image-text models. In *Thirty-Sixth Conference on Neural Information Processing Systems Datasets and Benchmarks Track*, October 2022.
- Sharir, O., Peleg, B., and Shoham, Y. The Cost of Training NLP Models: A Concise Overview, April 2020.
- Simonyan, K. and Zisserman, A. Very deep convolutional networks for large-scale image recognition. In Bengio, Y. and LeCun, Y. (eds.), *Proc. of ICLR*, 2015.
- Verma, V., Lamb, A., Beckham, C., Najafi, A., Mitliagkas, I., Lopez-Paz, D., and Bengio, Y. Manifold Mixup: Better

- Representations by Interpolating Hidden States. In *ICML*, 2019.
- Vetterli, M. and Herley, C. Wavelets and Filter Banks: Theory and Design. *IEEE Transactions on Signal Processing*, 40(9):2207–2232, October 1992. doi: 10.1109/78.157221.
- Wang, Y., Huang, H., Rudin, C., and Shaposhnik, Y. Understanding How Dimension Reduction Tools Work: An Empirical Approach to Deciphering t-SNE, UMAP, TriMap, and PaCMAP for Data Visualization. *Journal of Machine Learning Research*, 22(201):1–73, 2021.
- Yang, K., Qinami, K., Fei-Fei, L., Deng, J., and Rusakovsky, O. Towards Fairer Datasets: Filtering and Balancing the Distribution of the People Subtree in the ImageNet Hierarchy. In *Proceedings of the 2020 Conference on Fairness, Accountability, and Transparency*, pp. 547–558, January 2020. doi: 10.1145/3351095.3375709.
- Yun, S., Han, D., Chun, S., Oh, S. J., Yoo, Y., and Choe, J. CutMix: Regularization strategy to train strong classifiers with localizable features. In *IEEE/CVF International Conference on Computer Vision, ICCV*, pp. 6022–6031, 2019. doi: 10/ghfg25.
- Zagoruyko, S. and Komodakis, N. Wide Residual Networks. In *Proceedings of the British Machine Vision Conference 2016, BMVC*, 2016.
- Zhang, H., Cissé, M., Dauphin, Y. N., and Lopez-Paz, D. Mixup: Beyond empirical risk minimization. In *Proc. of ICLR*, 2018.
- Zhong, Z., Zheng, L., Kang, G., Li, S., and Yang, Y. Random erasing data augmentation. In *The Thirty-Fourth AAAI Conference on Artificial Intelligence, AAAI*, pp. 13001–13008, 2020.
- Zhu, J.-Y., Park, T., Isola, P., and Efros, A. A. Unpaired Image-to-Image Translation Using Cycle-Consistent Adversarial Networks. In *IEEE International Conference on Computer Vision, ICCV*, pp. 2242–2251, Venice, October 2017. IEEE. ISBN 978-1-5386-1032-9. doi: 10/gfhw33.